

Inadequacies of the Fisher Information Matrix in gravitational-wave parameter estimation

Carl L. Rodriguez,^{1,*} Benjamin Farr,^{1,†} Will M. Farr,^{1,‡} and Ilya Mandel^{2,§}

¹*Center for Interdisciplinary Exploration and Research in Astrophysics (CIERA) & Dept. of Physics and Astronomy, Northwestern University, 2145 Sheridan Rd, Evanston, IL 60208, USA*

²*School of Physics and Astronomy, University of Birmingham, Edgbaston, Birmingham, B15 2TT*

The Fisher Information Matrix (FIM) has been the standard approximation to the accuracy of parameter estimation on gravitational-wave signals from merging compact binaries due to its ease-of-use and rapid computation time. While the theoretical failings of this method, such as the signal-to-noise ratio (SNR) limit on the validity of the lowest-order expansion and the difficulty of using non-Gaussian priors, are well understood, the practical effectiveness compared to a real parameter estimation technique (e.g., Markov-chain Monte Carlo) remains an open question. We present a direct comparison between the FIM error estimates and the Bayesian probability density functions produced by the parameter estimation code `lal inference mcmc`. In addition to the low-SNR issues usually considered, we find that the FIM can greatly overestimate the uncertainty in parameter estimation achievable by the MCMC. This was found to be a systematic effect for systems composed of binary black holes, with the disagreement increasing with total mass. In some cases, the MCMC search returned standard deviations on the marginalized posteriors that were smaller by several orders of magnitude than the FIM estimates. We conclude that the predictions of the FIM do not represent the capabilities of real gravitational-wave parameter estimation.

I. INTRODUCTION

By 2015, the first generation of gravitational wave detectors capable of detecting astrophysical sources will become operational [1–3]. Beyond the first detection, the science promise of these instruments lies in the ability to estimate the parameters of the generating sources from their data. Much of the literature outlining the scientific potential of advanced generation detectors, particularly with respect to the coalescence of compact binaries, has focused on the parameter estimation capabilities [e.g. 4, 5]. These studies have informed both the design and science goals of ground-based interferometer networks.

When discussing parameter estimation, a distinction must be made between theoretical predictions for parameter-estimation accuracy and the actual techniques used to measure said parameters. For most theoretical applications, the standard approach has been the Fisher Information Matrix (FIM), a well-known tool from statistics that has been adapted to gravitational-wave signal analysis [6, 7]. Computing the FIM requires only the partial derivatives of an analytic gravitational-wave signal model. It can be shown that, in the strong-signal limit, the inverse of the FIM is the variance-covariance matrix of the estimated signal parameters. That is, the inverse of the FIM gives a first-order estimate of how well one could, in theory, measure the parameters of a given system. This estimate also corresponds to the Cramer-Rao bound on the variance of an unbiased estimator for the parameters.

This is in contrast to the actual techniques used in parameter estimation, in which one calculates the overlap of the detector output with theoretical templates of gravitational-wave signals [8, 9]. Since most realistic waveform templates are generated from a high-dimensional parameter space, the difficulty lies in adequately sampling this space. Several studies have been performed using the LIGO-Virgo Collaboration code, `lal inference mcmc`, to develop a uniform framework for Bayesian inference on gravitational-wave data using multiple sampling algorithms [e.g. 10]. One common sampling technique, Markov-Chain Monte Carlo (MCMC), has proved to be particularly efficient [e.g. 11, 12].

An MCMC study explores the full parameter space, with fixed data; the FIM explores the space of data at fixed parameters. This global MCMC exploration of the full parameter space can, in some cases, yield highly multi-modal, non-Gaussian posterior probability distributions which vary substantially from the uncertainties predicted by the FIM. Given the effective difference between these two techniques, and the prospect of real gravitational-wave detections and parameter estimation within the next few years [1, 2, 13, 14], the question naturally arises: how well do the theoretical estimates provided by the Fisher Matrix formalism compare to those achievable in practice with an MCMC search? In this paper, we attempt to answer that question by directly comparing the standard deviations from MCMC searches to the estimates generated by the FIM. We confirm the standard assumption that the Fisher Matrix is invalid at low signal-to-noise ratios; however, we also find that the FIM fails at high signal strengths for systems with a total mass greater than $10M_{\odot}$. In those cases, the Markov-Chain Monte Carlo is constraining parameters much more accurately than the FIM estimates.

These results robustly confirm the discrepancy first

* cr@u.northwestern.edu

† bfarr@u.northwestern.edu

‡ w-farr@northwestern.edu

§ ilyamandel@chgk.info

noted by Cokelaer [15] in the context of real parameter estimation. In several ways, this paper serves as an experimental confirmation of the warnings given by Vallisneri [16]: that the Fisher Matrix cannot and should not be used without several checks of internal consistency. In section II, we review the basic analytic setup for parameter estimation of gravitational-wave signals. We review the Fisher Matrix formalism in section II A, and then describe specific details of the parameter estimation code in II B. We present the primary results in section III. Finally, in section IV, we explore various causes for the breakdown of the FIM, including the unexpected effects of prior boundaries parameters (IV A), the breakdown of the linear-signal approximation (IV B), the necessity of averaging over many noise realizations for a fair comparison (IV C), and the potential influence of hidden estimator bias (IV D), explored through a reduced-dimensionality test case. Although we speculate on several plausible causes, we do not yet have a fully convincing explanation for this breakdown of the Cramer-Rao bound. Throughout the paper, we assume $G = c = 1$, and employ the summation convention over repeated indices. In Appendices A, B, and C we review the derivation of the Cramer-Rao bound, its application to situations with a hard boundary in the data-generating distribution, and its application to systems with strong prior constraints or boundaries.

II. PARAMETER ESTIMATION

We begin by introducing a Bayesian formalism for parameter estimation. We assume that the time-domain output of a gravitational-wave detector can be written as an additive combination of nature's gravitational waveform h_0 and the noise of the detector n . We further assume that this noise is stationary and Gaussian with mean zero. With these assumptions the detector output is

$$s = n + h_0. \quad (1)$$

We can write the probability of a specific data realization s conditioned on the waveform parameters, $\boldsymbol{\theta}$, as a Gaussian probability density of the residuals once the waveform h has been subtracted,

$$\begin{aligned} p(s|\boldsymbol{\theta}) &\propto \exp\left[-\frac{1}{2}\langle n|n\rangle\right] \\ &= \exp\left[-\frac{1}{2}\langle s - h(\boldsymbol{\theta})|s - h(\boldsymbol{\theta})\rangle\right]. \end{aligned} \quad (2)$$

Here $\boldsymbol{\theta}$ is the set of parameters for the template waveform, not the parameters of the actual signal, h_0 , which we refer to as $\boldsymbol{\theta}_0$. The inner product, $\langle | \rangle$, is defined using the noise spectrum of the detectors as

$$\langle a|b\rangle \equiv 4\Re \int df \frac{\tilde{a}(f)\tilde{b}^*(f)}{S_n(f)}, \quad (3)$$

where $S_n(f)$ is the one-sided power spectral density of the noise as a function of frequency, and $\tilde{a}(f)$ and $\tilde{b}(f)$ are the Fourier transforms of the time-domain signals $a(t)$ and $b(t)$.

Once we have the likelihood of the detector output (2), we employ Bayes Rule to obtain the posterior probability of the system parameters $\boldsymbol{\theta}$ given the output s as

$$\begin{aligned} p(\boldsymbol{\theta}|s) &= \frac{p(\boldsymbol{\theta})p(s|\boldsymbol{\theta})}{p(s)} \\ &\propto p(\boldsymbol{\theta}) \exp\left[-\frac{1}{2}\langle s - h(\boldsymbol{\theta})|s - h(\boldsymbol{\theta})\rangle\right], \end{aligned} \quad (4)$$

where $p(\boldsymbol{\theta})$ are the prior probabilities of the source parameters and $p(s)$ is a normalization constant. The prior information can come either from physical limits in the parameter space, or from a priori knowledge of astrophysical systems. If we pick a set of parameters $\boldsymbol{\theta} \approx \boldsymbol{\theta}_0$ such that $h(\boldsymbol{\theta}) \approx h_0$, then the posterior (4) will be near a global maximum; however, the presence of noise will in general deflect the maximum of the posterior away from $\boldsymbol{\theta}_0$. That is, in the presence of noise, there is no guarantee that the posterior is maximized at the true parameters of the system. The goal of parameter estimation is to sample the available parameter space, considering all areas of posterior support, to determine the posterior probability density function on the parameters of the signal. We will discuss one such sampling technique, Markov-Chain Monte Carlo, in Section II B.

A. Fisher Information Matrix

With the above machinery in place, the Fisher Matrix can be motivated as follows. Expand the template about the $\boldsymbol{\theta}_0$ waveform as

$$h(\boldsymbol{\theta}) = h_0 + \Delta\theta^i h_i \dots \quad (5)$$

where the h_i are the partial derivatives with respect to the i^{th} parameter, evaluated at the true values, and $\Delta\theta^i = \theta^i - \theta_0^i$. Truncation at first-order in the partial derivatives is sometimes referred to as the linearized-signal approximation (LSA). Inserting equations (5) and (1) into the posterior probability (4) yields the LSA posterior probability distribution:

$$\begin{aligned} p(\boldsymbol{\theta}|s) &\propto p(\boldsymbol{\theta}) \exp\left[-\frac{1}{2}\langle n|n\rangle + \right. \\ &\quad \left. \Delta\theta^k \langle n|h_k\rangle - \frac{1}{2}\Delta\theta^i \Delta\theta^j \langle h_i|h_j\rangle\right] \end{aligned} \quad (6)$$

Note that the posterior is a probability distribution over parameters $\boldsymbol{\theta}$ conditioned on the detector output, s . Vallisneri [16, §IIE] shows that the LSA is equivalent to the leading term of the posterior expanded as a series in $\epsilon \equiv 1/\text{SNR}$. It is for this reason that we treat the LSA as applicable in the high-SNR regime.

Calculations with Eq. (6) are simplest when using “flat” priors, $p(\boldsymbol{\theta}) \sim \text{const.}$ Even if the prior is not strictly independent of $\boldsymbol{\theta}$, if the scale on which the prior changes is much larger than the scale over which the posterior varies, the prior can be approximated as a constant. Under the flat-prior assumption, the mean of $\Delta\theta^i$ is

$$\langle \Delta\theta^i \rangle \equiv \frac{\int d\boldsymbol{\theta} \Delta\theta^i p(\boldsymbol{\theta}|s)}{\int d\boldsymbol{\theta} p(\boldsymbol{\theta}|s)} = (\langle h_i|h_j \rangle)^{-1} \langle n|h_j \rangle \quad (7)$$

and the covariance matrix of $\Delta\theta^i$ is

$$\begin{aligned} \text{cov}(\Delta\theta) &\equiv \langle (\Delta\theta^i - \langle \Delta\theta^i \rangle) (\Delta\theta^j - \langle \Delta\theta^j \rangle) \rangle \\ &= (\langle h_i|h_j \rangle)^{-1} \end{aligned} \quad (8)$$

These quantities are both formally conditioned on the data realization (i.e. the particular noise in s), though the covariance of $\Delta\theta$ is independent of n in the LSA.

Instead of using the Bayesian framework in Eq. (6), suppose we employ a maximum-likelihood estimator for the parameters $\Delta\theta^i$ under the LSA. Note that the likelihood is a distribution on the data conditioned on the parameters, so this is in some sense a reversal of the viewpoint in Eq. (6). The parameters that maximize the likelihood for fixed data are

$$\Delta\theta_{\text{ML}}^i(n) = (\langle h_i|h_j \rangle)^{-1} \langle n|h_j \rangle \quad (9)$$

Thus, under the LSA and a flat prior, the mean lies at the peak (mode) of the posterior. The expectation of the maximum likelihood estimator for $\Delta\theta^i$ over many data realizations with fixed parameters is

$$\langle \Delta\theta_{\text{ML}}^i(n) \rangle_n = \langle (\langle h_i|h_j \rangle)^{-1} \langle n|h_j \rangle \rangle_n = 0, \quad (10)$$

where we have used the notation $\langle \rangle_n$ to emphasize that this expectation is taken over the distribution of signals (i.e. noise realizations) with fixed parameters, in contrast to the angle brackets in Eqs. (7) and (8) which are taken over parameters with fixed data. Note that the expected value of the maximum-likelihood estimator for $\Delta\theta^i$ implies that the expected value of the maximum-likelihood estimator for $\boldsymbol{\theta}$ is $\boldsymbol{\theta}_0$, so this estimator is unbiased.

The covariance of the maximum-likelihood estimator for $\Delta\theta$ in the LSA is

$$\text{cov}_n(\Delta\theta_{\text{ML}}) = (\langle h_i|h_j \rangle)^{-1}, \quad (11)$$

where again we have used a subscript to indicate that the average here is over detector outputs at fixed parameters (i.e. noise realization). Comparing to Eq. (8), we see that the covariance of the maximum-likelihood estimator (under the distribution of noise) and the covariance of the parameters (under the Bayesian posterior with flat priors) are equal in the LSA (this equality is discussed at length in Vallisneri [16]).

The quantity $\langle h_i|h_j \rangle$ is also the Fisher information matrix (FIM) for the likelihood in Eq. (2):

$$F_{ij} \equiv - \langle \partial_i \partial_j \log p(s|\boldsymbol{\theta}) \rangle_n |_{\boldsymbol{\theta}=\boldsymbol{\theta}_0} = \langle h_i|h_j \rangle, \quad (12)$$

where we used Eq. (2), noting that the average over different noise realizations implies $\langle \langle a|n \rangle \langle n|b \rangle \rangle_n = \langle a|b \rangle$, and ignoring the contribution from the prior. The definition of the FIM does not depend on the LSA, but under the LSA we see that the covariances of both the maximum-likelihood estimator and the parameters under the posterior are equal to the inverse of the FIM.

When we consider the exponential form of (6) and that the $\Delta\theta^i$ are the displacements of the waveform parameters from the best-fit values of $\boldsymbol{\theta}_0$, we can then treat (6) as a multidimensional Gaussian with variance-covariance $\Sigma^{ij} = (F^{-1})^{ij}$. The standard deviations and cross-correlations of parameters are given by

$$\sigma_i = \sqrt{\Sigma^{ii}} \quad (13)$$

$$\text{cov}(\theta^i, \theta^j) = \frac{\Sigma^{ij}}{\sqrt{\Sigma^{ii}\Sigma^{jj}}} \quad (14)$$

1. Fisher Matrix as the Cramer-Rao Bound

One must be careful when discussing the full interpretation of the Fisher information matrix, as there are two separate statistical meanings of F_{ij} . The first, outlined above, is that in the high-SNR/LSA limit the FIM represents the inverse of the variance-covariance matrix. Under this interpretation, one assumes that for sufficiently loud waveforms, the posterior (4) becomes a true Gaussian, and that Σ^{ij} describes the uncertainties associated with the posterior for any fixed data realization¹. In this limit, we expect that the uncertainties returned by parameter estimation will coincide with those predicted by the FIM.

However, there is a second, equally valid interpretation of F_{ij} that is frequently employed: the inverse Fisher matrix gives the Cramer-Rao bound on the expected variance of any unbiased estimator for $\boldsymbol{\theta}_0$ over repeated measurements at fixed $\boldsymbol{\theta}_0$ (i.e. averaged over noise realizations). Recall that the Cramer-Rao bound is given by [16, 17]

$$|\Sigma^{ij}| \geq |\Sigma_{CR}^{ij}| \equiv |F_{ij}^{-1}| = \langle h_i|h_j \rangle^{-1}. \quad (15)$$

We give a derivation of the one-dimensional Cramer-Rao bound in Appendix A. Equation (15) is the same form of the covariance matrix that was stated in equations (8) and (11). However, the key difference is that, through the lens of the Cramer-Rao bound, (15) is now the lower bound on the covariance of unbiased parameter estimates that can be measured given the waveform h_0 , not the estimated errors that can be obtained in the high-SNR/LSA

¹But note that there is an additional “uncertainty” in the posterior due to the displacement of the peak from the true parameters, $\boldsymbol{\theta}_0$, which is given in Eq. (7). Under the LSA, this displacement has zero expectation under repeated data realizations and covariance equal to Σ^{ij} .

limit. We remind the reader that this implies the standard deviations obtained from the FIM are the *lower limit* on what is achievable on average from an unbiased estimator.

A subtle point is that the Cramer-Rao bound does not actually bound the variance of the Bayesian posterior in a trivial way, as we shall now describe. Recall that the Cramer-Rao bound applies to an unbiased estimator of the signal parameters, θ_0 , under repeated data realizations. Choose as an estimator for θ_0 a fair draw from the posterior, $\hat{\theta} \sim p(\theta|s)$. We will assume for the moment that the posterior is an unbiased estimator for θ_0 ; this is certainly true under the LSA (see Eq.(7)). The mean of this estimator over many data realizations with fixed θ_0 is the mean over θ and data realizations of the posterior:

$$\langle \hat{\theta} \rangle_n = \int ds \int d\theta \theta p(\theta|s) p(s|\theta_0). \quad (16)$$

The covariance of this estimator is

$$\text{cov}_n \hat{\theta} = \int ds \int d\theta \left(\theta^i - \langle \hat{\theta}^i \rangle_n \right) \left(\theta^j - \langle \hat{\theta}^j \rangle_n \right) \times p(\theta|s) p(s|\theta_0). \quad (17)$$

A bit of algebra reveals that two terms contribute to the covariance of $\hat{\theta}^2$:

$$\text{cov}_n \hat{\theta} = \text{cov}_n (\langle \theta \rangle) + \langle \text{cov} \theta \rangle_n. \quad (20)$$

The first term reflects the covariance under repeated data realizations of the posterior mean, while the second is the average under repeated data realizations of the posterior covariance. Informally, the former accounts for the shifting of the posterior peak, while the latter accounts for the typical posterior width. Together, they must satisfy the Cramer-Rao bound:

$$\text{cov}_n \hat{\theta} = \text{cov}_n (\langle \theta \rangle) + \langle \text{cov} \theta \rangle_n \geq \Sigma_{CR}^{ij}. \quad (21)$$

Another estimator for the true parameters, θ_0 , is the posterior mean, $\hat{\theta} = \langle \theta \rangle$. If a draw from the posterior is an unbiased estimator for θ_0 then so is the posterior mean. The Cramer-Rao bound for this estimator therefore implies

$$\text{cov}_n (\langle \theta \rangle) \geq \Sigma_{CR}^{ij}. \quad (22)$$

²Note the distinction between cov and cov_n . The cov_n operator is defined in Eq. (17), and involves an integral over the noise (i.e. data) distribution. The cov operator involves an integral over the posterior distribution for the parameter θ , and is defined by

$$\text{cov} \theta \equiv \int d\theta (\theta^i - \langle \theta^i \rangle) (\theta^j - \langle \theta^j \rangle) p(\theta|s), \quad (18)$$

with

$$\langle \theta \rangle \equiv \int d\theta \theta p(\theta|s). \quad (19)$$

Because covariance matrices are positive definite³, Eq. (22) implies Eq. (21) independently of the value of $\langle \text{cov} \theta \rangle_n$, so Eq. (21) does not constrain the posterior variance.

Though we have not proven that there is no bound on the mean posterior variance under the noise distribution induced by the Cramer-Rao bound, the argument above is suggestive that the Cramer-Rao bound does not apply to the variance of the posterior in a trivial way. Of course, since the posterior mean must have a variance under repeated signal realizations that is greater than the inverse Fisher matrix, in a consistent analysis the posterior variance should be of the same order on average. We will give several examples throughout the paper where the posterior variance is smaller than the inverse Fisher matrix.

In the above, we have been ignoring the effect of the prior, $p(\theta)$. For parameters that are tightly-constrained by the likelihood this is justified; however, for likelihoods that are wide enough that the prior changes appreciably over the region of significant likelihood support or that approach a hard boundary in the prior, the approach above is invalid. In general, an approach to a prior boundary introduces bias in estimators of θ derived from the posterior, so the unbiased Cramer-Rao bound no longer need apply. Several of the examples we show below where the full analysis significantly betters the Cramer-Rao bound have parameters that place significant posterior support near a prior boundary. In Appendix C, we use a toy example to illustrate the effect of hard boundaries in the prior on the Cramer-Rao bound.

When computing (12), it is important to carefully account for potential numerical errors, both from the numerical derivatives and from the matrix inversion required to produce (12). Our implementation and its numerical checks are described in section III C of [18]. Our numerical derivatives in (12) are computed with a 8th order finite difference scheme with an adaptive step size designed to minimize numeric error. Furthermore, these results were checked (for the intrinsic parameters) against an analytic computation of the derivatives, and successfully reproduce many well known results in the literature [4, 5, 16].

The inversion of (12) can pose a problem if the Fisher matrices are ill-conditioned (that is, their determinant is sufficiently close to zero that rounding errors become evident in the matrix inversion). However, we note here that the condition numbers (the ratio of the largest to small-

³Recall that the matrix statement

$$\mathbf{A} \geq \mathbf{B} \quad (23)$$

is to be interpreted as

$$\forall \mathbf{v}, \mathbf{v}^T \mathbf{A} \mathbf{v} \geq \mathbf{v}^T \mathbf{B} \mathbf{v}, \quad (24)$$

or, in other words, that $\mathbf{A} - \mathbf{B}$ is positive semi-definite.

est eigenvalues of F) of the majority (97%) of the results quoted here are below the inversion limit, which is approximately 10^{15} for a 64-bit infrastructure. In addition to this, we studied the stability of the LU inversion of the FIM with the largest condition number, (7.7×10^{15}), by perturbing the Γ entries at the decimal point of the largest derivative error and observing the effect on the inverse. In that case, the difference in the entries of the variance-covariance matrix were found to be negligible. Furthermore, the low-dimensional tests quoted in Table III were inverted with a smallest condition number of 2×10^7 , several orders of magnitude below the regime of numerical error. To summarize, we are confident in the full FIM results presented here.

B. Parameter estimation via Markov-Chain Monte Carlo

We use a Bayesian parameter estimation code, `lalinference_mcmc`, which is an enhancement of the previously described MCMC parameter estimation code `SpinSpiral` [8, 19]. It is designed to record a chain of samples whose distribution is $p(\boldsymbol{\theta}|s)$. The basic description of the Markov-Chain Monte Carlo via the Metropolis-Hastings algorithm is as follows [20]:

1. Pick an initial point in the parameter space ($\boldsymbol{\theta}_{\text{old}}$), and then propose a random “jump” to a new set of waveform parameters, $\boldsymbol{\theta}_{\text{new}}$. The jump follows the (conditional) jump probability distribution $q(\boldsymbol{\theta}_{\text{new}}|\boldsymbol{\theta}_{\text{old}})$.
2. Calculate the posterior probability, $p(\boldsymbol{\theta}_{\text{new}}|s)$, of the new parameters using (2) and (4).
3. Accept the new parameters with probability

$$p_{\text{accept}} = \min \left[1, \frac{p(\boldsymbol{\theta}_{\text{new}}|s)q(\boldsymbol{\theta}_{\text{old}}|\boldsymbol{\theta}_{\text{new}})}{p(\boldsymbol{\theta}_{\text{old}}|s)q(\boldsymbol{\theta}_{\text{new}}|\boldsymbol{\theta}_{\text{old}})} \right]. \quad (25)$$

If the new parameters are accepted, record $\boldsymbol{\theta}_{\text{new}}$ and repeat with $\boldsymbol{\theta}_{\text{old}} \leftarrow \boldsymbol{\theta}_{\text{new}}$; otherwise, record $\boldsymbol{\theta}_{\text{old}}$, and repeat.

Depending on the jump proposal distribution, q , the convergence (mixing) of the Markov chain may be rapid or slow. We employ multiple optimization techniques, including both specially-crafted q and parallel tempering, to ensure adequate mixing of the Markov Chains throughout the parameter space. The details of the algorithm can be found in [8, 19, 21].

The MCMC has been subjected to a series of tests to validate posterior estimates returned by the code. The estimates of several 15-dimensional analytic functions, including unimodal and bimodal correlated Gaussian distributions and Rosenbrock functions, have been tested against analytic functions using the Kolmogorov–Smirnov (KS) test. The same set of two hundred injections used for this study (generated from the prior

distribution) was also used to verify that the estimated Bayesian credible intervals correspond to the appropriate frequentist confidence intervals. This was done by calculating the quantile value at the true location for each parameter in each injection in the set. The distribution of quantiles for each parameter was then tested for uniformity, also using KS tests.

C. Signal Model

We use a frequency domain waveform accurate to 2^{nd} post-Newtonian (pN) order in phase. We restrict ourselves to quasi-circular waveforms as a simplifying assumption. The standard form of the waveform model, known as the TaylorF2 approximant, is calculated via the stationary phase approximation where the amplitude terms are truncated to leading order in frequency [22]. In this setup, the gravitational-wave amplitude is given by

$$\tilde{h}(f) = Af^{-7/6}e^{i\psi(f)}, \quad (26)$$

where $A \propto \mathcal{M}_c^{5/6}\Theta(\text{angle})/D$, D is the luminosity distance of the binary, and $\psi(f)$ is the pN phase. $\Theta(\text{angle})$ is a function of the orientation of the binary with respect to the detector network in terms of the sky position, orbital inclination, and the wave polarization. In addition to the binary component masses m_1 and m_2 , it is convenient to work with the total mass, $M \equiv m_1 + m_2$, the symmetric mass ratio η , and the chirp mass \mathcal{M}_c , defined by

$$\eta \equiv m_1 m_2 / M^2 \quad \text{and} \quad \mathcal{M}_c = \eta^{3/5} M. \quad (27)$$

Then, in terms of the Newtonian orbital velocity $v = (\pi M f)^{1/3}$, the 2pN phase is

$$\psi(f) = 2\pi f t_c - \phi_0 + \frac{\pi}{4} + \frac{3}{128\eta} v^{-5} \sum_{k=0}^4 \alpha_k v^k \quad (28)$$

with coefficients

$$\begin{aligned} \alpha_0 &= 1 \\ \alpha_1 &= 0 \\ \alpha_2 &= \frac{20}{9} \left(\frac{743}{336} + \frac{11}{4}\eta \right) \\ \alpha_3 &= -16\pi \\ \alpha_4 &= 10 \left(\frac{3058673}{1016064} + \frac{5249}{1008}\eta + \frac{617}{144}\eta^2 \right). \end{aligned} \quad (29)$$

The terms t_c and ϕ_0 in equation (28) are constants of integration, referring to the time and phase at coalescence, respectively. Although generally uninteresting physically, they must be accounted for in any parameter estimation study of the waveform phase.

For the TaylorF2 approximant, the standard amplitude is given in equation (26). However, the LALInspirational package included in the LSC Algorithm Library [23], which

generated the waveforms for our Markov-Chain Monte Carlo analysis, uses a non-standard definition of the amplitude. This causes a slight difference in the amplitude at high frequencies compared to the standard TaylorF2 waveform. This issue was also noted, but not accounted for, in the previous study by Coeklear [15]. We correct this discrepancy by using the same waveform for both the MCMC and FIM analyses. This was done purely for consistency, as in practice the waveform amplitude has a minimal effect on parameter estimation for non-spinning systems.

To perform the integral defined in (3), we used an analytic noise curve roughly representative of initial LIGO sensitivity, provided in [24], which takes the form:

$$S_h(f) = S_0 \left[\left(\frac{4.49f}{f_0} \right)^{-56} + \left(\frac{0.16f}{f_0} \right)^{-4.52} + 0.52 + 0.32 \left(\frac{f}{f_0} \right)^2 \right], \quad (30)$$

where $f_0 = 150$ Hz, and $S_0 = 9 \times 10^{-46} \text{Hz}^{-1}$. We consider the complete initial detector network consisting of the two LIGO sites (in Hanford, WA and Livingston, LA) and the Virgo site (in Pisa, Italy), although for simplicity we use the Initial LIGO sensitivity for all three detectors. For a multi-detector network, the likelihood $p(s|\boldsymbol{\theta})$ is a product of the likelihoods $p(s_{det}|\boldsymbol{\theta})$ over individual detectors, allowing us to use the above formalism with minimal modification. We integrate the inner product from a lower frequency cutoff of 40Hz to the innermost-stable-circular orbit of the system in question, which for a non-spinning binary is given by

$$\pi f_{\text{ISCO}} = \frac{1}{6^{3/2} M}. \quad (31)$$

In addition to the intrinsic parameters (\mathcal{M}_c, η) and phasing parameters (ϕ_0, t_c) listed above, we include an additional 5 extrinsic parameters in the waveform model in order to explore how a complete study on real data, including parameters such as sky location, will compare to their FIM counterparts. This leads to a 9-dimensional parameter space for non-spinning systems:

$$\boldsymbol{\theta} = (\mathcal{M}_c, \eta, \phi_0, t_c, D, \iota, \psi, \alpha, \delta) \quad (32)$$

where D is the luminosity distance to the binary, ι is the orbital inclination, ψ is the gravitational-wave polarization, and α and δ are the right ascension and declination of the source on the sky.

The optimal matched-filter signal-to-noise ratio (SNR) of a gravitational wave in a single detector is

$$\rho \equiv \frac{4}{\sigma} \int_0^\infty df \frac{|\tilde{s}(f)\tilde{h}^*(f)|}{S_n(f)} \quad (33)$$

where ρ is the SNR and $\tilde{s}(f)$ and $\tilde{h}(f)$ are the frequency-domain signal and template, respectively. The SNRs for

multiple detectors add in quadrature. The normalization σ , corresponding to the standard deviation of the matched filter output when applied to noise alone, is given by

$$\sigma^2 = 4 \int_0^\infty df \frac{|\tilde{h}(f)|^2}{S_n(f)}. \quad (34)$$

For the MCMC analysis, we compute the SNR directly using (33). In the case of the FIM, we approximate the SNR using σ from equation (34) for a network of detectors as

$$\rho = \sqrt{\sum_i \sigma_i^2} \quad (35)$$

where the index i refers to the data of the i^{th} detector. It should be noted that equations (33)–(35) are only valid in case of stationary Gaussian noise.

III. RESULTS

To quantify the difference between the uncertainty estimates on individual parameters, we use the uncertainty fraction,

$$\Lambda \equiv \frac{\sigma^{\text{FIM}}}{\sigma^{\text{MCMC}}}. \quad (36)$$

where σ^{FIM} is the standard deviation predicted by the Fisher matrix and σ^{MCMC} is the standard deviation of the posterior distribution. An uncertainty fraction near unity indicates that the FIM estimate and MCMC standard deviation agree, whereas a value less than unity indicates the FIM uncertainty is smaller than the MCMC uncertainty, while values above unity indicate that the MCMC standard deviation is smaller than the FIM estimate.

We simulate 200 random, non-spinning systems using the TaylorF2 waveform described in section II C. For the MCMC, we inject the signals into randomly generated noise realizations using simulated Initial LIGO Gaussian noise, (30). The source distribution, which was then employed as the prior distribution by the MCMC, $p(\boldsymbol{\theta})$, is:

- uniform in component masses in $1M_\odot \leq m_1, m_2 \leq 15M_\odot$, with a total-mass cutoff of $M \leq 20M_\odot$;
- uniform in the logarithm of luminosity distance, $\log(D)$, with a range of $10 \text{ Mpc} \leq D \leq 40 \text{ Mpc}$; and
- uniform in all other parameters.

We plot the uncertainty fraction, Λ , for each of the 9 parameters in our waveform model. The results for intrinsic and phasing parameters are shown in Figure 1. The results for the extrinsic parameters are shown in Figure 2.

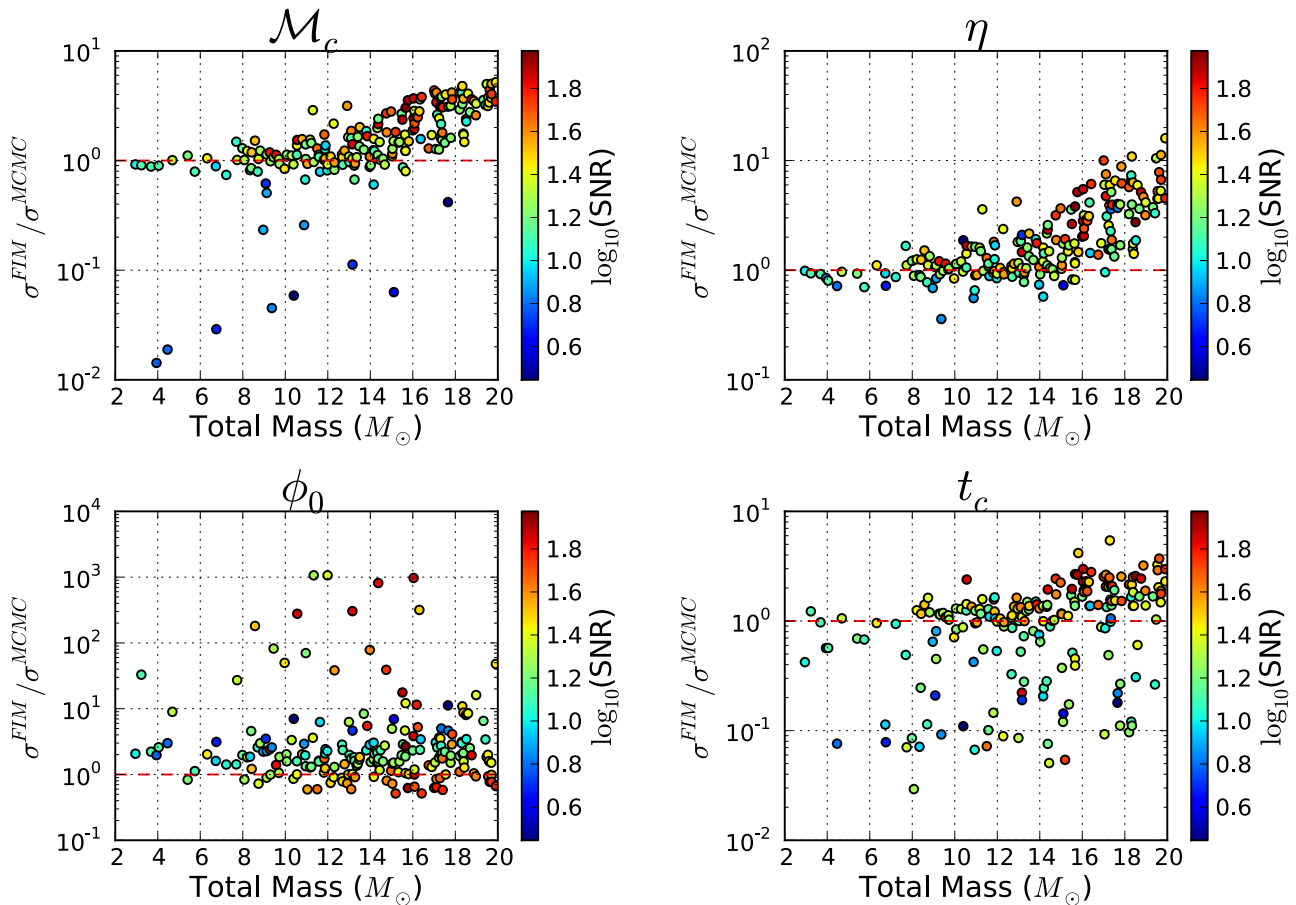


FIG. 1. The fractional difference between the marginalized FIM and MCMC standard deviations of the intrinsic and phasing parameters as a function of total system mass. The color bar illustrates the $\log_{10}(\text{SNR})$ of the injection, while the red line at unity represents agreement between the FIM and MCMC errors. Note in particular the systematic divergence at $M > 10M_{\odot}$ in the two mass parameters \mathcal{M}_c and η . Also note that the uncertainties in ϕ_0 can often be severely overestimated by the FIM.

We focus first on the two mass parameters, \mathcal{M}_c and η , as these are the intrinsic parameters of direct physical interest in most studies. Immediately, Fig. 1 reveals two distinct features. First, a sufficiently low SNR will cause the uncertainty fraction Λ to drop significantly below unity. In particular, points on the \mathcal{M}_c plot of Fig. 1 below $\rho \approx 8$ show a mismatch between the two techniques of several orders of magnitude in some cases.

The second feature is the systematic divergence of Λ above unity for systems with a high total mass. As the mass of the system increases, the MCMC analysis appears to return standard deviations smaller than those predicted by the FIM. At high masses ($\sim 20M_{\odot}$), the FIM can over-estimate the MCMC standard deviations by a factor of 4 in chirp mass, and more than a factor of 10 in η . The large (30) number of points above $18M_{\odot}$, all with $\Lambda > 1$, suggest the effect is neither a fluke of the parameter space nor due to a specific realization of the noise, but is in fact a systematic failure of the FIM to reliably estimate the posterior variance at high masses. We will explore the reasons for this discrepancy in Section IV.

Turning to the extrinsic parameters, there appears to be no distinct trend similar to that seen in the intrinsic parameters. For the errors in D , ι , and ψ , the FIM can over-estimate the standard deviations of the MCMC analysis by several orders of magnitude. For the luminosity distance, this is most likely due to the non-uniform shape of the prior probability distribution. The MCMC assumes a prior distance evenly distributed in $\log(D)$. For the inclination and wave polarization, the disparity between the FIM and MCMC results is likely due to how the two techniques are computing the posterior. The MCMC is evaluating the full likelihood surface, in which waveforms at ι and $\iota + \pi$ are identical. This knowledge restricts the errors returned by the MCMC to (roughly) their physical limits (which, in the case of inclination, means the error will always be less than π radian). The FIM, meanwhile, is computed at a local point in parameter space, and does not have access to the knowledge that the likelihood function is periodic in certain parameters (see Section IV A). Furthermore, since inclination is highly correlated with luminosity distance, the non-uniform prior imposed by the MCMC on distance will

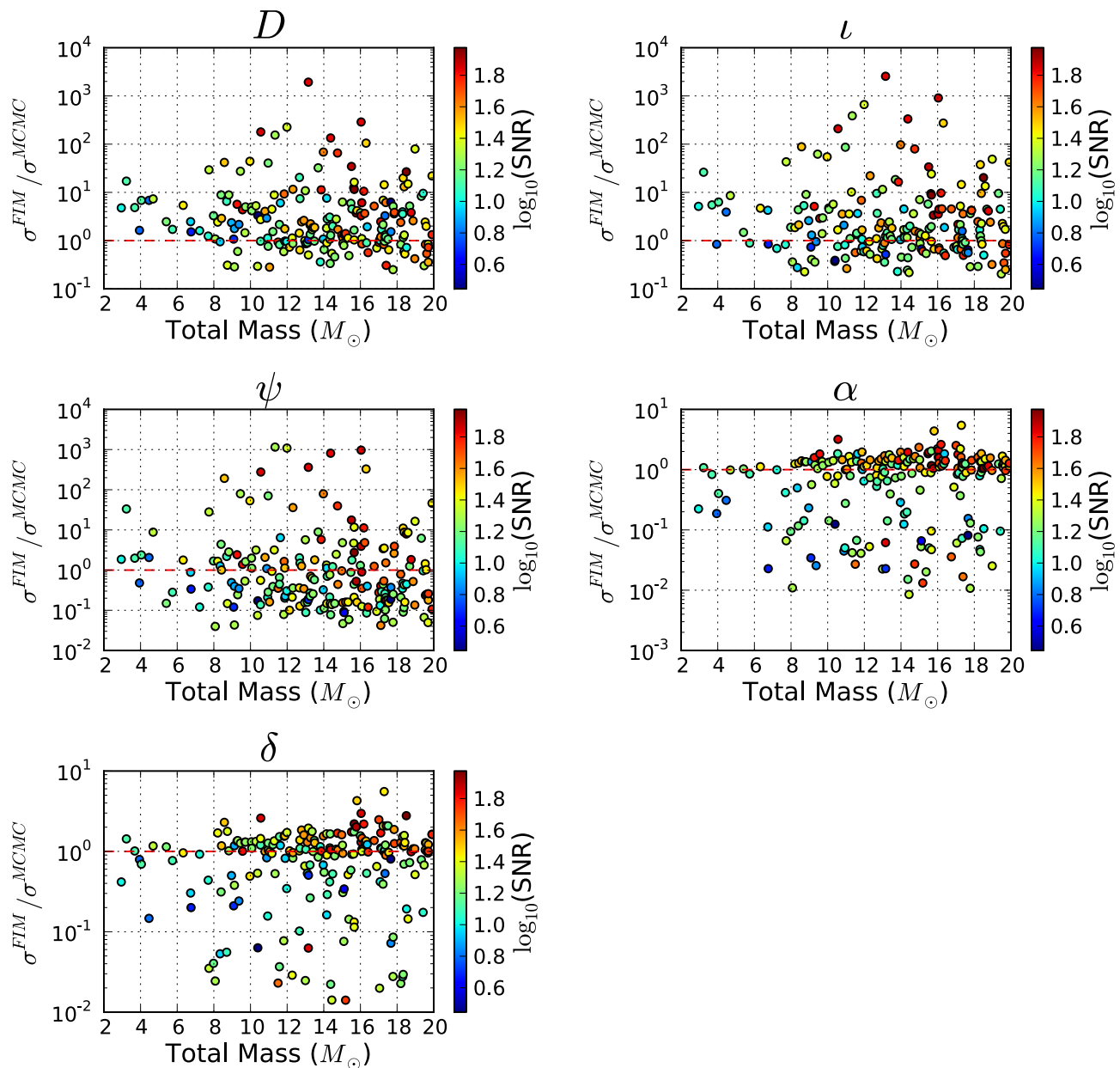


FIG. 2. The fractional difference between the marginalized FIM and MCMC standard deviations of the extrinsic parameters as a function of total system mass. Unlike the intrinsic parameters (Fig. 1), the uncertainty fraction does not depend on system mass.

affect the uncertainties in ι via the cross-correlation.

It is surprising that the FIM appears, at first glance, to provide an adequate error estimate for the sky location of the source. The average Λ for the sky angles α and δ is 0.97 and 1.00, respectively. Since the calculation of the Fisher Matrix includes the full three-detector network and the geocentric time-of-arrival difference (folded into t_c in equation (28) for each individual detector site), the FIM has access to the same amount of local information as the full MCMC. This does not mean that the FIM standard deviations for a single point in the sky-position parameter space can be trusted: for a single

point in the sky, several factors (multimodal probability distributions, non-Gaussian posteriors, etc.) can cause the FIM and MCMC standard deviations to disagree by up to three orders of magnitude. Furthermore, we note that the FIM tends to highly underestimate the error for the low-SNR cases, and slightly overestimate the error for the high-SNR cases (beginning at about $\rho = 25$). While this effect averages to unity for the current study, we note that this is obviously dependent on the distribution of source SNRs. As the set of injections were not distributed uniformly in volume, we expect that this result will not hold in general. However, as an ensemble aver-

TABLE I. The average normalized cross-correlations between the two mass parameters and the two “junk” intrinsic parameters. Note in particular the high median correlations with coalescence phase ϕ_0 . This allows unphysical uncertainties in coalescence phase (those larger than 2π) to bias mass estimate uncertainties when evaluated using the FIM.

Correlation	Mean	Median
$ C(\mathcal{M}_c, \phi_0) $	0.66	0.88
$ C(\mathcal{M}_c, t_c) $	0.72	0.78
$ C(\eta, \phi_0) $	0.69	0.93
$ C(\eta, t_c) $	0.78	0.85

age, the results indicate that the FIM can be useful for large scale studies comparing the sky-localization abilities of various detector configurations and designs (e.g. [10]).

IV. BREAKDOWN OF THE FISHER MATRIX

Having demonstrated the existence of a systematic issue with the Fisher Matrix uncertainty estimates, we now explore potential causes of the high-mass disagreement between the FIM and MCMC standard deviations. We analyze a few of the possible situations that can arise when using the Fisher Matrix, and attempt to quantify which of these are causing the discrepancy in the presented results.

A. The Problem of Priors and Restricted Parameters

One issue of the Fisher Matrix formalism is the restriction of the domain of (12) to \mathbb{R}^n . In reality, of course, several of our parameters in θ are angular (e.g. ϕ_0, ψ), and are restricted to \mathbb{S}^1 . For instance, the coalescence phase, ϕ_0 , can only take values in the range of 0 to 2π , and usually has a flat posterior. Since the Fisher Matrix is attempting to fit a Gaussian distribution on \mathbb{R}^1 to a uniform distribution on \mathbb{S}^1 , standard deviations on ϕ_0 can reach into the thousands of radians. Given that the coalescence phase tends to be highly correlated with the chirp mass (see Table I), it is inevitable that some of the unreasonably large uncertainties calculated for ϕ_0 would induce unphysically large deformations of the \mathcal{M}_c and η error ellipses. Appendix C gives a toy example illustrating how the general effect of bounded priors is to introduce bias into the estimator, rendering the unbiased Cramer-Rao bound inappropriate.

To test the effects of these unphysical standard deviations on our parameters of interest, we rerun the FIM over the injection points with a Gaussian prior of width $\sigma_{\phi_0}^{\text{prior}} = 2\pi$. A Gaussian prior can be easily incorporated into the Fisher matrix [5, 16]; more complicated

priors cannot. The results for the intrinsic parameters are shown, alongside the flat prior results, in Fig. 3. Adding a prior on ϕ_0 to the FIM analysis decreases, but does not correct, the divergence between the FIM and MCMC estimates in the high-mass, high-SNR regime. Although a more restrictive prior might remove the divergence completely (the $\sigma_{\phi_0}^{\text{prior}} = 2\pi$ prior still allows significant support outside the $[0, 2\pi]$ allowed range for ϕ_0), there is no physical justification for such a restriction.

However, it is important to point out that $\phi_0 \in [0, 2\pi]$ priors are used in MCMC calculations only for the sake of speed. Very wide priors could be used instead, and while the marginalized posterior on the coalescence phase would obviously change, the marginalized posterior on chirp mass would be unaffected. That is because waveforms with $\phi_0 \rightarrow \phi_0 + 2n\pi$ are identical and have identical likelihoods as computed in the MCMC. Therefore, it is not obvious that these compact, angular parameters are really to blame for the apparent violation of the Cramer-Rao bound.

We have only considered a prior on coalescence phase because ϕ_0 is the only angular parameter in the 9-dimensional model that is strongly correlated with the two mass parameters. Priors on extrinsic parameters, while useful for those parameters, were found to have a minimal effect on the mass parameters. Therefore, prior information on sky position, inclination, distance, etc. does not translate en masse to the errors on \mathcal{M}_c and η , since the cross-correlations between those parameters are relatively insignificant.

A potentially more problematic prior is the physical boundary at $\eta = 0.25$ in the mass parameter space. If, for instance, a signal were to have injected parameters at $\eta = 0.25$, the standard deviations returned by the FIM would range to unphysical values of the mass ratio. The MCMC errors suffer no such drawback as they are not limited to Gaussian-only posteriors. It is then reasonable to assume that the mass-ratio cutoff has influenced all of the FIM results quoted in Figures 1 and 3.

As stated above, there is no simple way to include non-Gaussian prior information in the Fisher-matrix formalism. However, the majority of our 200 signals (65%) were selected with sufficiently asymmetric mass ratios such that the $1\text{-}\sigma$ surface about the injected values returned by the FIM did not exceed the physical boundary at $\eta = 0.25$. We conclude that while an exact prior would affect the results, the overall trend itself cannot be explained by a prior boundary; otherwise, some of the high-mass points (those whose $1\text{-}\sigma$ boundaries were completely physical) in the \mathcal{M}_c and η plots of Fig. 1 would lie at unity, which is not observed. Additionally, the previous study by Cokelaer [15] attempted to correct this issue by removing the boundary at $\eta = 0.25$ in their Monte Carlo parameter estimation. Even when η was allowed to assume nonphysical values, it was found that the FIM still returned uncertainties larger than those generated by a full parameter-estimation search.

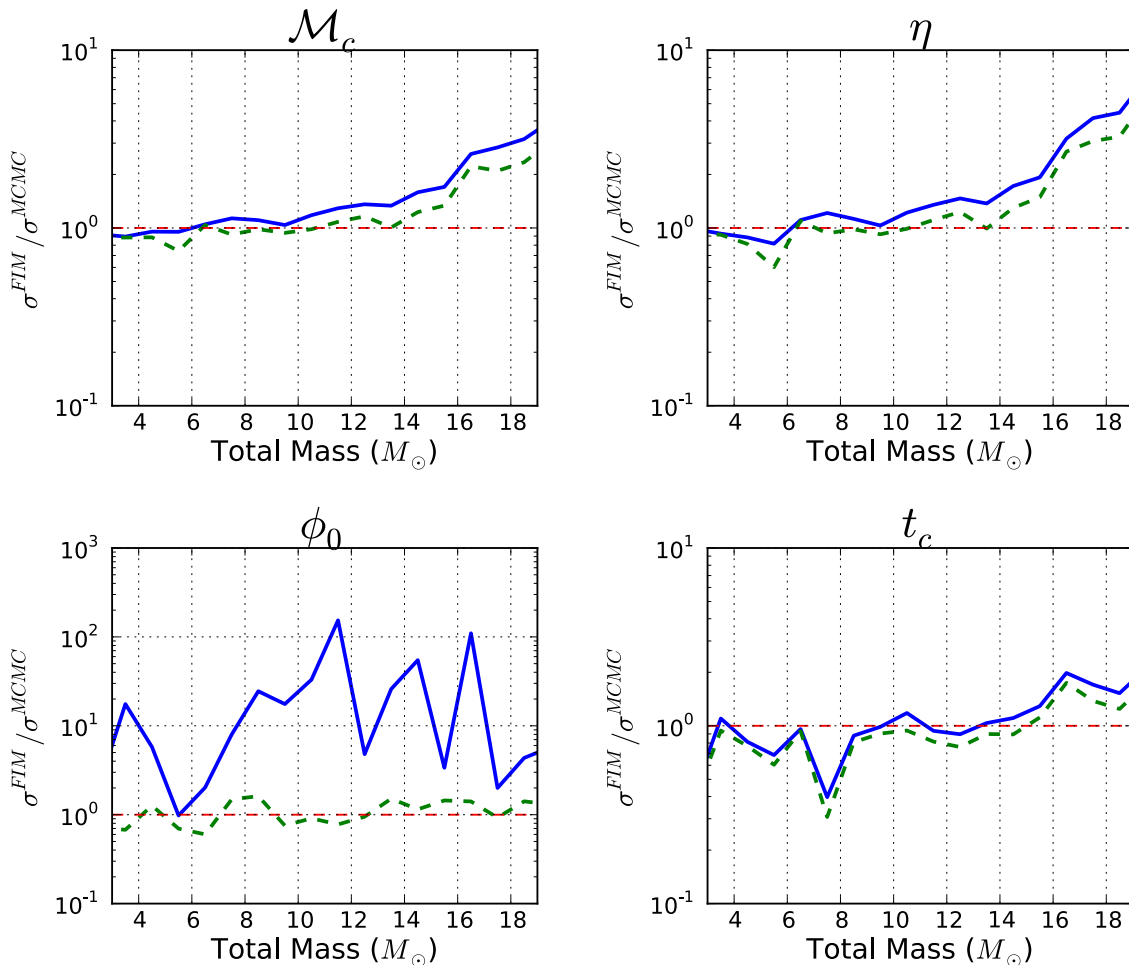


FIG. 3. The averaged fractional differences between the FIM and MCMC standard deviations, Λ , for FIM runs with and without a Gaussian prior on ϕ_0 (dashed green and solid blue, respectively). We have averaged the points with a bin size of $1M_\odot$ in order to better illustrate the difference between the two datasets. Points with SNRs below $\rho = 10$ have been excluded. The phase prior clearly lowers the FIM estimates of uncertainties on other parameters due to the high correlations; however, the effect is only one contribution to the high mass divergence of σ_{FIM} and σ_{MCMC} .

In general, an MCMC analysis will out-perform the Cramer-Rao bound when the posterior probability is significantly truncated by any boundaries in a non-Gaussian prior. For the initial results reported in section III, the MCMC was performed with a maximum component mass of $m_{1,2} \leq 15M_\odot$, and a total mass of $m_1 + m_2 \leq 20M_\odot$, in addition to the $\eta \leq 0.25$ restriction. Given the population of samples, some of which are injected close to these boundaries, there are some systems whose MCMC posteriors encounter the prior boundaries. Were the Fisher Matrix to be evaluated in component-mass parameters in these regions, the corresponding $1\text{-}\sigma$ surfaces would also extend beyond these boundaries (a fact which is encoded in the $1\text{-}\sigma$ values for \mathcal{M}_c and η in this study). However, when considering all possible prior boundaries, we find that at least 33% of the 27 MCMC results with a total mass greater than $18M_\odot$ do not possess significant probability support near these mass cutoffs. We

conclude that while the choice of prior has affected the results quoted here, it cannot completely explain the divergence observed in Figure 1. In Section IV D, we perform an analysis with no prior boundaries in the total or component masses, the results of which solidify this claim.

B. Breakdown of the LSA

Although it does not explain the observed violation of the Cramer-Rao bound, the breakdown of the linear-signal approximation at low SNRs can provide a clear example of when the FIM results should be treated as suspect. Vallisneri [16] developed a criterion to determine if the SNR of a single signal was sufficiently loud for the LSA to be considered valid. By comparing the difference between two nearby evaluations of the waveform

to the linearized shift in the waveform, $\theta^i h_i(\boldsymbol{\theta}_0)$, one can quantify how valid the LSA is for a specific $\boldsymbol{\theta}_0$ and SNR. In this case, the differences are computed between the waveform at the true value and at a random point on the $1\text{-}\sigma$ surface, $\Delta h = h(\boldsymbol{\theta}_0 + \boldsymbol{\sigma}) - h(\boldsymbol{\theta}_0)$. The overlap of the residuals, r , is defined as

$$|\log(r)| \equiv \langle \theta^i h_i - \Delta h | \theta^j h_j - \Delta h \rangle / 2 \quad (37)$$

By computing this overlap ratio for a large number of points distributed over the $1\text{-}\sigma$ surface predicted by the FIM, the ratio $\log(r)$ provides an estimate of how linearized the waveform is at that point in parameter space. Furthermore, since the size of the $1\text{-}\sigma$ surface depends on the signal SNR, (37) can be used to determine the linearity of a waveform as a function of SNR, and therefore how appropriate the FIM is for a given system.

We applied the Vallisneri criterion to each of the 200 signals presented above, by computing the overlap of 1000 points evenly distributed on each $1\text{-}\sigma$ surface. Following [16], a particular system was considered to be in the linear regime if $|\log(r)| \leq 0.1$ for 90% of the points. While the criterion is both intuitive and useful, we found that the majority of systems failed the consistency check. This held true even for the low-mass points where the FIM and MCMC estimates agreed. We concluded that the criterion provides a sufficient but not necessary check of the self-consistency of the Fisher Matrix.

C. The Necessity of Averaging over Many Noise Realizations

The MCMC and Fisher-matrix analyses address different statistical ensembles. The MCMC analysis treats the data as fixed, and the parameters are allowed to vary; the Fisher analysis treats the parameters as fixed and the data as random. Thus, it is expected that the two methods will not agree for the analysis of any one signal. However, when an average is taken over many different signal realizations (parameter choices) and data (noise choices), the results should be on average consistent with each other in the appropriate limits. We believe that we have enough analyses with different noise and parameter values that the trend towards higher errors at higher masses observed in Section III is robust. As a check, we selected two injections with total masses of $3.2M_\odot$ and $19.7M_\odot$, and ran the MCMC on data corresponding to these signals with 5 distinct noise realizations. The results are shown in Fig. 4. As expected, the points do display a spread in values when the noise realization of the MCMC is changed. However, the spread is substantially narrower than the distance above unity for the high-mass system; we conclude that the upward trend in Fig. 1 is robust.

We have also observed the same trend in a Fisher matrix analysis when the FIM is computed at the empirical maximum-likelihood parameters found in the MCMC

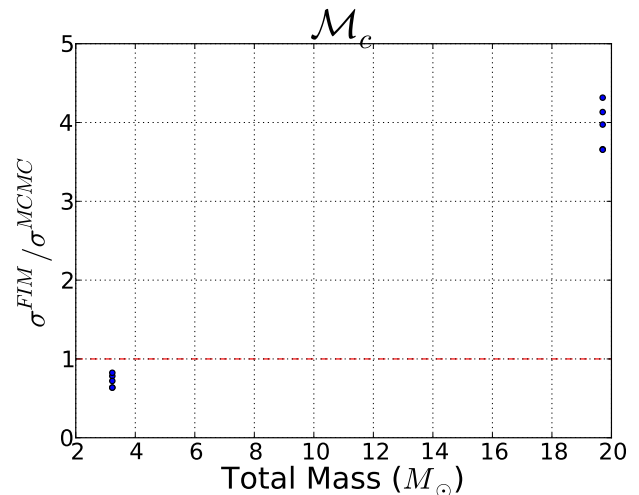


FIG. 4. The fractional difference between the FIM and MCMC standard deviations of the chirp mass as a function of total system mass for two points with total masses $3.2M_\odot$ and $19.7M_\odot$. The two systems were selected with parameters at least $1\text{-}\sigma$ away from any prior boundary (as measured by the FIM), and with no significant posterior support near the same prior boundaries (as measured by the MCMC). The vertical spread represents different MCMC standard deviations taken from runs with identical parameters with different randomly generated realizations of the detector noise. Note how the low-mass points are all below unity, suggesting the FIM is providing an adequate lower bound, while the high-mass points are all in substantial disagreement with the MCMC predictions, even allowing for differences from specific noise realizations.

analysis, rather than at the ‘true’ injected parameters. This served to exclude the first source of noise-based covariance (the displacement of the mean) identified in (20). The results are consistent with the Fisher matrix analysis at the true parameters $\boldsymbol{\theta}_0$; we list the change in the average standard deviations in Table II.

D. Hidden Prior Bias

The Cramer-Rao bound as stated applies to only unbiased estimators of a parameter. But the bound in Eq. (12) only incorporates information from the likelihood, while the MCMC analysis uses the posterior, which includes a prior distribution, $p(\boldsymbol{\theta})$.

By default, the uniform priors on the component masses `lal_inference_mcmc` employs yield highly non-flat priors in \mathcal{M}_c and η . In effect, our choice of prior may provide a biased estimator with which we could surpass the Cramer-Rao bound. As a final test of the results, we reduce the comparison to the simplest possible case. We choose a low-mass and high-mass injection from the 200 injections. Both systems were selected with a sufficiently asymmetric mass ratio to ensure no interference from the physical cutoff at $\eta = 0.25$. To remove any possible bias

TABLE II. Mean and median uncertainty fractions for the 200 injections, with the FIM evaluated at the injected parameters versus the maximum likelihood point of the MCMC. For the two mass parameters, the average change in standard deviation is negligible. The only parameters to exhibit a large shift are the mean values for ψ and ϕ_0 . This is due to the presence of outliers, and does not appear to affect estimation of the other parameters on average.

Parameter	Λ_{Inject}	Λ_{MaxL}	Λ_{Inject}	Λ_{MaxL}
	Mean		Median	
\mathcal{M}_c	1.84	1.82	1.43	1.39
η	2.43	2.37	1.49	1.43
ϕ_0	29.67	211.24	1.96	1.43
t_c	1.20	1.20	1.14	1.16
D	20.65	11.82	2.06	0.91
ι	32.79	43.23	1.67	0.71
ψ	29.57	211.67	0.46	0.22
α	0.97	0.94	1.04	0.98
δ	1.00	0.97	1.00	1.00

and correlations, we employ uniform priors in the MCMC

$$p(\mathcal{M}_c) = 1 \quad 0.8M_\odot \leq \mathcal{M}_c \leq 10M_\odot \quad (38)$$

$$= 0 \quad \text{otherwise}$$

$$p(\eta) = 1 \quad 0.05 \leq \eta \leq 0.25 \quad (39)$$

$$= 0 \quad \text{otherwise}$$

and reduce the MCMC to a two-dimensional space over only the mass parameters \mathcal{M}_c and η , with all other parameters held fixed at their true values. This choice of priors also eliminates the issue of boundaries in total and component masses discussed in Section IV A. We then performed an MCMC on the two injections into 50 different realizations of Gaussian noise, thus enabling a valid comparison between the spread of the MCMC estimators and the standard deviations returned by the FIM. For the reduced dimensionality runs, we find near perfect agreement between the standard deviation of the MCMC estimates and the Cramer-Rao bound for both mass cases. We also find support for the claim that the average of the uncertainty estimates of the individual MCMC experiments equals the standard deviation of posterior means over multiple noise realizations. See Table III.

As a test of our hypothesis in section IV A, we then perform the same analysis over a three-dimensional parameter space consisting of the two mass parameters and the chirp phase (\mathcal{M}_c , η , and ϕ_0). In this case, we find that the MCMC matches the uncertainty estimates predicted by the FIM for the low-mass system. For the high mass system, the MCMC still produces standard deviations which significantly surpass the Cramer-Rao bound in all three parameters when ϕ_0 is included as a free parameter. The results are illustrated in Table III. Notice that for the 3-D case, the uncertainties in ϕ_0 for both the low and high mass systems are substantially less than 2π .

This seems to suggest that the 2π domain of ϕ_0 (and indeed all other angular parameters) cannot be responsible for the breakdown of the Cramer-Rao bound in this context. When one adds the coalescence phase parameter into the analysis, the FIM begins to noticeably fail in the high-mass regime. To test whether this effect is due to bias in the \mathcal{M}_c estimator, we use the biased form of the Cramer-Rao bound given in [16]:

$$\Sigma_{il}^{\text{biased}} \equiv (\delta_{im} + \partial_m b_i(\boldsymbol{\theta}_0)) \Sigma_{mj}^{CR} (\delta_{jl} + \partial_j b_l(\boldsymbol{\theta}_0)) \quad (40)$$

where $b_i(\boldsymbol{\theta}_0)$ is the bias of the estimator in the i^{th} parameter, evaluated at the true parameters (see Appendix A for a derivation of the biased Cramer-Rao bound). In order for any bias from the boundary in ϕ_0 to influence the bound on \mathcal{M}_c , for instance, the MCMC estimator would need to have non-zero first derivatives of the chirp mass bias $b_{\mathcal{M}_c}(\boldsymbol{\theta}_0)$. Since the recovery of the posterior in the 2-dimensional case appears consistent with the Cramer-Rao bound, it is reasonable to assume that the two mass parameters are individually unbiased, such that $\partial_{\mathcal{M}_c} b_{\mathcal{M}_c}(\boldsymbol{\theta}_0) = \partial_\eta b_{\mathcal{M}_c}(\boldsymbol{\theta}_0) = 0$. Therefore, the only source of chirp mass bias must arise from the $\partial_{\phi_0} b_{\mathcal{M}_c}(\boldsymbol{\theta}_0)$ term. Under that assumption, along with the symmetry of Σ and equation (40), the biased Cramer-Rao bound on \mathcal{M}_c in the 3-dimensional model becomes

$$\begin{aligned} \Sigma_{\mathcal{M}_c \mathcal{M}_c}^{\text{biased}} = & \Sigma_{\mathcal{M}_c \mathcal{M}_c}^{CR} + 2\Sigma_{\mathcal{M}_c \phi_0}^{CR} \partial_{\phi_0} b_{\mathcal{M}_c}(\boldsymbol{\theta}_0) \\ & + \Sigma_{\phi_0 \phi_0}^{CR} (\partial_{\phi_0} b_{\mathcal{M}_c}(\boldsymbol{\theta}_0))^2 \end{aligned} \quad (41)$$

We can approximate the derivative as

$$\partial_{\phi_0} b_{\mathcal{M}_c}(\boldsymbol{\theta}_0) \rightarrow \frac{b_{\mathcal{M}_c}(\phi_0) - b_{\mathcal{M}_c}(\phi_0 - \sigma_{\phi_0}^{FIM})}{\sigma_{\phi_0}^{FIM}} \quad (42)$$

using the 1- σ FIM errors on ϕ_0 as a natural derivative length scale for the problem. We calculate $b_{\mathcal{M}_c}$ using the mean of the MCMC posteriors as our estimator. $b_{\mathcal{M}_c}(\phi_0 - \sigma_{\phi_0}^{FIM})$ is calculated similarly by performing a second set of 50 MCMC runs with parameters displaced in ϕ_0 by $\sigma_{\phi_0}^{FIM}$. Performing this test, we find that the chirp mass estimator is not significantly biased by our choice of ϕ_0 (Table IV). We conclude that the MCMC estimator is sufficiently unbiased.

Previous studies have observed similar ‘‘violations’’ of the Cramer-Rao bound [15, 25], as well as a similar agreement between the FIM and the likelihood for a two-dimensional model [26]. Furthermore, Vallisneri [16] and Cutler & Flanagan [7] point out that the Cramer-Rao bound is often unhelpful in practice due to the effects of estimator bias. We have speculated on several possible explanations for the apparent breakdown of the Cramer-Rao bound. However, despite exploring a variety of possibilities, we have not been able to find a completely convincing explanation for this behavior.

TABLE III. Comparisons of the statistical uncertainty between the FIM and MCMC for the limited dimensionality, flat prior tests for low-mass and high-mass systems. The MCMC errors for the two systems are reported as two separate values. $\sigma_{\text{mean}}^{\text{MCMC}}$ is the frequentist standard deviation of the means, calculated by considering the mean of each MCMC posterior as the output of an estimator and computing the standard deviation of that estimator. $\text{Mean}(\sigma^{\text{MCMC}})$ is the mean of the Bayesian posterior standard deviations, computed by averaging the standard deviation of each MCMC posterior. The FIM uncertainties σ^{FIM} are also presented. The 2-D problem estimates only the mass parameters, \mathcal{M}_c and η , while the 3-D problem also includes ϕ_0 . In the 2-D problem, the low-mass system obeys the Cramer-Rao bound, and the high-mass system is very nearly within the Cramer-Rao bound. In the 3-D problem the low-mass system obeys the Cramer-Rao bound, but in the high-mass system the MCMC standard deviations are below the Cramer-Rao lower bound.

Low Mass ($4.043M_\odot$)		2-D Problem (\mathcal{M}_c and η)			3-D Problem (\mathcal{M}_c , η , and ϕ_0)		
Parameter	Injected Value	$\sigma_{\text{mean}}^{\text{MCMC}}$	$\text{Mean}(\sigma^{\text{MCMC}})$	σ^{FIM}	$\sigma_{\text{mean}}^{\text{MCMC}}$	$\text{Mean}(\sigma^{\text{MCMC}})$	σ^{FIM}
\mathcal{M}_c	1.650	8.17×10^{-5}	8.09×10^{-5}	8.04×10^{-5}	2.03×10^{-4}	1.64×10^{-4}	1.62×10^{-4}
η	0.2244	1.97×10^{-4}	1.84×10^{-4}	1.83×10^{-4}	1.05×10^{-3}	8.34×10^{-4}	8.25×10^{-4}
ϕ_0	2.38	–	–	–	0.178	0.142	0.141
High Mass ($18.20M_\odot$)		2-D Problem (\mathcal{M}_c and η)			3-D Problem (\mathcal{M}_c , η , and ϕ_0)		
Parameter	Injected Value	$\sigma_{\text{mean}}^{\text{MCMC}}$	$\text{Mean}(\sigma^{\text{MCMC}})$	σ^{FIM}	$\sigma_{\text{mean}}^{\text{MCMC}}$	$\text{Mean}(\sigma^{\text{MCMC}})$	σ^{FIM}
\mathcal{M}_c	6.257	2.57×10^{-3}	2.72×10^{-3}	2.73×10^{-3}	5.88×10^{-3}	5.46×10^{-3}	7.07×10^{-3}
η	0.169	2.38×10^{-4}	2.66×10^{-4}	2.68×10^{-4}	1.34×10^{-3}	1.22×10^{-3}	1.66×10^{-3}
ϕ_0	5.32	–	–	–	0.147	0.164	0.194

TABLE IV. \mathcal{M}_c errors for the high-mass, 3-dimensional system (bottom right column of Table III), but employing (40) to correct the bias present in the maximum likelihood estimator from the compact domain of ϕ_0 . Although the biased Cramer-Rao bound ($\sigma_{\text{biased}}^{\text{FIM}}$) is smaller than its unbiased counterpart ($\sigma_{\text{unbiased}}^{\text{FIM}}$), it is still larger than the MCMC standard deviations.

Error Type	$\sigma_{\mathcal{M}_c} (\times 10^{-3} M_\odot)$
$\sigma_{\text{mean}}^{\text{MCMC}}$	5.88
$\sigma_{\text{unbiased}}^{\text{FIM}}$	7.07
$\sigma_{\text{biased}}^{\text{FIM}}$	6.81

V. CONCLUSION

In this paper we compared the parameter estimation capabilities of one of the Bayesian codes used by the LIGO Scientific Collaboration, `lal inference_mcmc`, to the theoretical estimates provided by the Fisher Information Matrix. The purpose was to compare the effectiveness of previous FIM predictions to the accuracy achievable with real parameter estimation techniques that will be employed once the Advanced LIGO/VIRGO network begins to regularly detect signals from compact binary coalescence. Many studies have used the Fisher information to describe the science capabilities of advanced detectors; our analysis provides a route to understanding what these studies imply about the actual parameter estimation uncertainties when making inference on signals from compact binary coalescences.

We found two distinct effects in the uncertainties of the two mass parameters. For low-SNR signals, the FIM can produce standard deviations several orders of magnitude

smaller those realizable by an MCMC search. This is expected, since the Fisher Matrix as an LSA approximation is based on an expansion in $1/\text{SNR}$, and requires a sufficiently loud source for the linear-signal approximation to be valid. However, we also discovered a systematic divergence between the FIM and MCMC uncertainties for signals with a total mass above $\sim 10M_\odot$. Beyond $16M_\odot$ for \mathcal{M}_c and $18M_\odot$ for η , all of our injected signals were recovered by the MCMC with tighter uncertainties than the FIM would suggest possible. This effect was noted for signals with distinct noise realizations, and with a wide range of “reasonable” SNRs from $\rho \approx 10$ to $\rho \approx 100$.

We checked several possible causes for this discrepancy, including correlations with unconstrained parameters (e.g. ϕ_0), the displacement of the MCMC maximum likelihood from the injected parameters, and possible bias from our choice of priors. We found a slight improvement in FIM estimates by adding a constraint on ϕ_0 , but even with this (weak) constraint the overall effect persisted. We conclude that the breakdown is a systematic error potentially affecting all FIM predictions, or at least those using frequency-domain waveforms above $10M_\odot$. This calls into question several previous parameter-estimation predictions in the literature [e.g., 4, 5, 18]. A full parameter estimation study (currently underway) will be required to determine the true capabilities of Advanced LIGO/VIRGO, particularly when constraining the masses of binary black hole systems. It should also be noted that, while we employed the Initial LIGO noise curve here (for computational convenience in the MCMC analysis), the systematic nature of the trend indicates a potential issue with any known implementation of the Fisher Matrix analysis [e.g., 25], and should lend caution to all future studies.

We also found that the FIM estimates of the extrin-

sic parameters (D , ι , ψ , α , δ) were highly variable. For the luminosity distance, inclination, and wave polarization, the Fisher Matrix standard deviations were found to vary wildly relative to those returned by the MCMC (with the ratios of standard deviations, Λ , varying by as much as 4 orders of magnitude). We also found that the FIM and MCMC uncertainties on sky-location angles, α and δ , disagreed by over 2 orders of magnitude in some cases; we also found that the Λ values for the sky-location parameters (α and δ) averaged to 1 over the 200 injected signals. However, this result may depend on the injection distribution, and should not be trusted in general.

New techniques are being developed which explore the parameter space more fully than the FIM, but without the complications of a full MCMC. By locally mapping the likelihood surface, these techniques (such as the exact mapping of the maximum likelihood estimator [27], or the fitting of an “Effective Fisher Matrix” via the local ambiguity function [28]), may avoid, or at least make apparent, the pitfalls we have outlined in this study.

We must still stress that any FIM study performed without these checks of the likelihood surface should not

be trusted blindly. It is entirely likely that the Fisher Information Matrix estimates could be failing, and that the failure is not producing an overly conservative lower-bound on the standard deviation, as has commonly been assumed, but is producing errors substantially worse than those realizable in practice. For cases such as these, one must employ a more robust technique which fully explores the posterior probability surface.

ACKNOWLEDGMENTS

We thank Michele Vallisneri, Patrick Brady, Frank Ohme, Vicky Kalogera, Cole Miller, Thomas Dent, Drew Keppel, and Alberto Vecchio for useful discussions. CR and BF were supported by NSF GRFP Fellowships, award DGE-0824162. WF and IM are grateful to the hospitality of the Kavli Institute for Theoretical Physics, where part of this work was carried out; it was supported in part by the National Science Foundation under Grant No. NSF PHY11-25915.

-
- [1] G. M. Harry and the LIGO Scientific Collaboration, *Classical Quant. Grav.* **27**, 084006 (2010).
 - [2] Virgo Collaboration, *Advanced Virgo Baseline Design*, Technical Report VIR-0027A-09 (2009).
 - [3] C. Cutler and K. S. Thorne, (2002), arXiv:gr-qc/0204090.
 - [4] K. G. Arun, B. R. Iyer, B. S. Sathyaprakash, and P. A. Sundararajan, *Phys. Rev. D* **71**, 084008 (2005), arXiv:gr-qc/0411146.
 - [5] E. Poisson and C. M. Will, *Phys. Rev. D* **52**, 848 (1995), arXiv:gr-qc/9502040.
 - [6] L. S. Finn, *Phys. Rev. D* **46**, 5236 (1992), arXiv:gr-qc/9209010.
 - [7] C. Cutler and É. E. Flanagan, *Phys. Rev. D* **49**, 2658 (1994), arXiv:gr-qc/9402014.
 - [8] V. Raymond, M. V. van der Sluys, I. Mandel, V. Kalogera, C. Röver, and N. Christensen, *Classical and Quantum Gravity* **27**, 114009 (2010), arXiv:0912.3746 [gr-qc].
 - [9] J. Veitch and A. Vecchio, *Phys. Rev. D* **81**, 062003 (2010), arXiv:0911.3820 [astro-ph.CO].
 - [10] J. Veitch, I. Mandel, B. Aylott, B. Farr, V. Raymond, C. Rodriguez, M. van der Sluys, V. Kalogera, and A. Vecchio, *Phys. Rev. D* **85**, 104045 (2012), arXiv:1201.1195 [astro-ph.HE].
 - [11] M. van der Sluys, V. Raymond, I. Mandel, C. Röver, N. Christensen, V. Kalogera, R. Meyer, and A. Vecchio, *Classical and Quantum Gravity* **25**, 184011 (2008), arXiv:0805.1689.
 - [12] M. V. van der Sluys, C. Röver, A. Stroeer, V. Raymond, I. Mandel, N. Christensen, V. Kalogera, R. Meyer, and A. Vecchio, *Astrophys. J. Lett.* **688**, L61 (2008), arXiv:0710.1897.
 - [13] J. Abadie, B. P. Abbott, R. Abbott, M. Abernathy, T. Accadia, F. Acernese, C. Adams, R. Adhikari, P. Ajith, B. Allen, and et al., *Classical and Quantum Gravity* **27**, 173001 (2010), arXiv:1003.2480 [astro-ph.HE].
 - [14] the LIGO Scientific Collaboration, the Virgo Collaboration, J. Aasi, J. Abadie, B. P. Abbott, R. Abbott, T. D. Abbott, M. Abernathy, T. Accadia, F. Acernese, and et al., *ArXiv e-prints* (2013), arXiv:1304.1775 [gr-qc].
 - [15] T. Cokelaer, *Classical and Quantum Gravity* **25**, 184007 (2008).
 - [16] M. Vallisneri, *Phys. Rev. D* **77**, 042001 (2008), arXiv:gr-qc/0703086.
 - [17] E. T. Jaynes, *Probability Theory: The Logic of Science* (Cambridge University Press, 2003).
 - [18] C. L. Rodriguez, I. Mandel, and J. R. Gair, *Phys. Rev. D* **85**, 062002 (2012), arXiv:1112.1404 [astro-ph.HE].
 - [19] M. van der Sluys, I. Mandel, V. Raymond, V. Kalogera, C. Röver, and N. Christensen, *Classical and Quantum Gravity* **26**, 204010 (2009), arXiv:0905.1323 [gr-qc].
 - [20] W. R. Gilks, *Markov Chain Monte Carlo In Practice* (Chapman and Hall/CRC, 1999).
 - [21] M. V. van der Sluys, C. Röver, A. Stroeer, V. Raymond, I. Mandel, N. Christensen, V. Kalogera, R. Meyer, and A. Vecchio, *Astrophys. J. Lett.* **688**, L61 (2008), arXiv:0710.1897.
 - [22] A. Buonanno, B. R. Iyer, E. Ochsner, Y. Pan, and B. S. Sathyaprakash, *Phys. Rev. D* **80**, 084043 (2009), arXiv:0907.0700 [gr-qc].
 - [23] “Lsc algorithm library (lal) software,” <http://www.lsc-group.phys.uwm.edu/lal>.
 - [24] T. Damour, B. R. Iyer, and B. S. Sathyaprakash, *Phys. Rev. D* **63**, 044023 (2001), arXiv:gr-qc/0010009.
 - [25] N. J. Cornish and E. K. Porter, *Classical and Quantum Gravity* **23**, 761 (2006), arXiv:gr-qc/0605085.
 - [26] D. Keppel, A. P. Lundgren, B. J. Owen, and H. Zhu, *ArXiv e-prints* (2013), arXiv:1305.5381 [gr-qc].

- [27] M. Vallisneri, Physical Review Letters **107**, 191104 (2011), arXiv:1108.1158 [gr-qc].
 [28] H.-S. Cho, E. Ochsner, R. O'Shaughnessy, C. Kim, and C.-H. Lee, ArXiv e-prints (2012), arXiv:1209.4494 [gr-qc].

Appendix A: The Cramer-Rao Bound

The Cramer-Rao bound limits the variance of an unbiased estimator of a function on a probability space obtained from a finite set of samples from this space. Let d be a set of samples drawn according to a parameterized probability distribution, $p(d|\theta)$:

$$d \sim p(d|\theta). \quad (\text{A1})$$

We want to estimate some function of θ , $\psi(\theta)$, using a function of the data, d ,

$$\psi(\theta) \simeq T(d). \quad (\text{A2})$$

We will assume that the estimator T is unbiased, that is

$$\langle T(d) \rangle_{p(d|\theta)} \equiv \int dd p(d|\theta) T(d) = \psi(\theta). \quad (\text{A3})$$

The quantity

$$s(d, \theta) \equiv \frac{\partial}{\partial \theta} \ln p(d|\theta) \quad (\text{A4})$$

is known as the score. As long as we can interchange the order of integration over d and differentiation with respect to θ , we can show that the expected value of the score is zero. We can interchange integration and differentiation when

1. The allowed range of d does not depend on θ and
2. Both $p(d|\theta)$ and $\partial p/\partial \theta$ are continuous and
3. If the allowed range of d is infinite (i.e. if the integral is improper), then all integrals must converge uniformly.

Under these conditions, we have $\langle s(\theta) \rangle_{p(d|\theta)} = 0$ by the following:

$$\begin{aligned} \langle s(d, \theta) \rangle_{p(d|\theta)} &= \int dd p(d|\theta) \frac{\partial}{\partial \theta} \ln p(d|\theta) \\ &= \int dd \frac{\partial}{\partial \theta} p(d|\theta) \\ &= \frac{\partial}{\partial \theta} \int dd p(d|\theta) \\ &= 0. \end{aligned} \quad (\text{A5})$$

We will assume that conditions 1, 2, and 3 hold unless otherwise noted.

Consider the covariance of the estimator T and the score:

$$\begin{aligned} \text{cov}(T, s) &= \\ &\left\langle \left(T(d) - \langle T(d') \rangle_{p(d'|\theta)} \right) \left(s(d, \theta) - \langle s(d', \theta) \rangle_{p(d'|\theta)} \right) \right\rangle_{p(d|\theta)} \end{aligned} \quad (\text{A6})$$

Since $\langle s(d, \theta) \rangle_{p(d|\theta)} = 0$, this reduces to

$$\begin{aligned} \text{cov}(T, s) &= \langle T(d) s(d, \theta) \rangle_{p(d|\theta)} \\ &= \int dd p(d|\theta) T(d) \frac{\partial}{\partial \theta} \ln p(d|\theta) \\ &= \int dd T(d) \frac{\partial}{\partial \theta} p(d|\theta) \\ &= \frac{\partial}{\partial \theta} \int dd T(d) p(d|\theta) \\ &= \frac{\partial}{\partial \theta} \psi(\theta). \end{aligned} \quad (\text{A7})$$

The Cauchy-Schwarz inequality requires

$$\text{cov}(T, T) \text{cov}(s, s) \geq (\text{cov}(T, s))^2, \quad (\text{A8})$$

so

$$\text{cov}(T, T) \geq \frac{(\partial \psi / \partial \theta)^2}{I(\theta)}, \quad (\text{A9})$$

where the Fisher information, $I(\theta)$, is defined to be the covariance of the score:

$$I(\theta) = \left\langle (s(d, \theta))^2 \right\rangle_{p(d|\theta)} = - \left\langle \frac{\partial^2}{\partial \theta^2} \ln p(d|\theta) \right\rangle_{p(d|\theta)}. \quad (\text{A10})$$

Eq. (A9) is the Cramer-Rao bound on the variance of the estimator T .

1. Biased Estimators

In the event that the estimator, $T(d)$, is biased, so that

$$\langle T(d) \rangle_{p(d|\theta)} = \psi(\theta) + b(\theta), \quad (\text{A11})$$

the Cramer-Rao bound is modified to

$$\text{cov}(T, T) \geq \frac{(\partial \psi / \partial \theta + \partial b / \partial \theta)^2}{I(\theta)}. \quad (\text{A12})$$

(See Eq. (A7).)

Appendix B: Bounded Data

Consider the probability distribution defined by

$$p_\epsilon(x) = \frac{1}{1 + \sqrt{2\pi}\epsilon} \begin{cases} \exp\left(-\frac{(x+\frac{1}{2})^2}{2\epsilon^2}\right) & x < -\frac{1}{2} \\ 1 & -\frac{1}{2} < x < \frac{1}{2} \\ \exp\left(-\frac{(x-\frac{1}{2})^2}{2\epsilon^2}\right) & x > \frac{1}{2} \end{cases} \quad (\text{B1})$$

Appendix C: Bounded Parameter

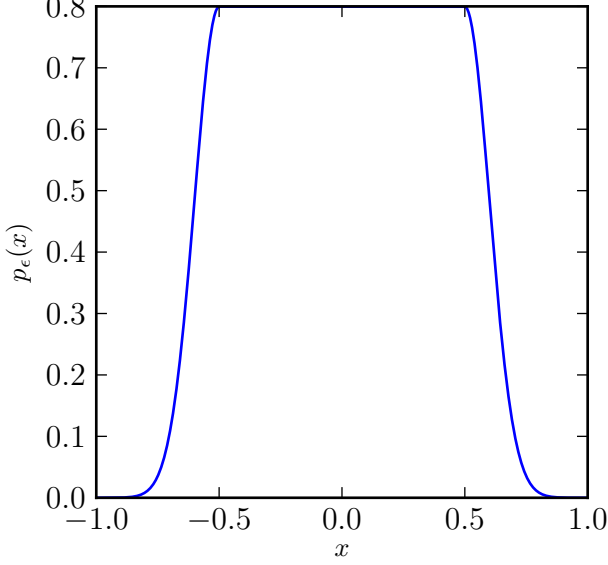


FIG. 5. The probability distribution $p_\epsilon(x)$ defined in Eq. (B1) with $\epsilon = 0.1$

A plot of this function appears in Figure 5. As $\epsilon \rightarrow 0$, the distribution goes over to a bounded, “top-hat” distribution between $-1/2$ and $1/2$, but the distribution is everywhere (twice) differentiable and nowhere zero for $\epsilon > 0$. This is required to satisfy conditions 1, 2, and 3 above.

Consider data produced from a parameter θ with noise drawn from p_ϵ :

$$d = \theta + X, \quad (\text{B2})$$

with

$$X \sim p_\epsilon(X). \quad (\text{B3})$$

As $\epsilon \rightarrow 0$, the data concentrate in the bounded range $\theta \pm 1/2$. The likelihood for these data is

$$p(d|\theta) = p_\epsilon(d - \theta). \quad (\text{B4})$$

Because our distribution is everywhere twice differentiable, we can compute the Fisher information. A little algebra reveals

$$I(\theta) = \frac{\sqrt{2\pi}}{\epsilon} \frac{1}{1 + \sqrt{2\pi}\epsilon}, \quad (\text{B5})$$

so the Cramer-Rao bound for estimators, $T(d)$, of $\psi(\theta)$ is

$$\text{cov}(T, T) \geq \frac{\epsilon}{\sqrt{2\pi}} \left(1 + \sqrt{2\pi}\epsilon\right) (\partial\psi/\partial\theta)^2. \quad (\text{B6})$$

As $\epsilon \rightarrow 0$, the Cramer-Rao bound for T becomes trivial. In other words, when the data generating distribution has a hard boundary the Fisher information becomes infinite and the Cramer-Rao bound becomes trivial.

Suppose we generate data from the following random process:

$$d = \theta + n, \quad (\text{C1})$$

with

$$n \sim N(0, \sigma), \quad (\text{C2})$$

where N is the normal distribution of width σ , and further suppose we have good prior information on θ , that is:

$$p(\theta) = U(-\epsilon, \epsilon), \quad (\text{C3})$$

where U is the uniform distribution. We wish to infer the value of θ using the data set d . The Bayesian posterior for θ after N observations of d is given by

$$p(\theta|d) = \begin{cases} \alpha \exp\left(-\sum_{i=1}^N \frac{(d_i - \theta)^2}{2\sigma^2}\right) \frac{1}{2\epsilon} & -\epsilon < \theta < \epsilon \\ 0 & \text{otherwise} \end{cases}, \quad (\text{C4})$$

where α is a normalizing constant. Suppose we want to estimate θ using the posterior mean:

$$\theta \simeq T(d) = \int d\theta \theta p(\theta|d). \quad (\text{C5})$$

After some algebra, we have

$$T(d) = \frac{D}{N} - \sqrt{\frac{2}{\pi}} \frac{\sigma}{\sqrt{N}} \frac{\exp\left(-\frac{(D-N\epsilon)^2}{2N\sigma^2}\right) - \exp\left(-\frac{(D+N\epsilon)^2}{2N\sigma^2}\right)}{\text{erf}\left(\frac{D+N\epsilon}{\sqrt{2N}\sigma}\right) - \text{erf}\left(\frac{D-N\epsilon}{\sqrt{2N}\sigma}\right)}, \quad (\text{C6})$$

where

$$D \equiv \sum_{i=1}^N d_i. \quad (\text{C7})$$

Because

$$\left\langle \frac{D}{N} \right\rangle_{p(d|\theta)} = \theta, \quad (\text{C8})$$

the estimator $T(d)$ is biased. As one might expect, when

$$\epsilon \gg \frac{\sigma}{\sqrt{N}}, \quad (\text{C9})$$

the second term in Eq. (C6) is small, and the estimator is approximately unbiased; in this limit, the width of the prior, 2ϵ , is large compared to the width of the posterior, which is approximately σ/\sqrt{N} . In the other limit, when

$$\epsilon \ll \frac{\sigma}{\sqrt{N}}, \quad (\text{C10})$$

we have

$$T(d) = \frac{D\epsilon^2}{3\sigma^2} + \mathcal{O}\left(\frac{\epsilon^4}{\sigma^4}\right), \quad (\text{C11})$$

whence

$$\langle T(d) \rangle_{p(d|\theta)} \simeq \frac{N\theta\epsilon^2}{3\sigma^2}. \quad (\text{C12})$$

In this case, the bias is

$$b(\theta) = \langle T(d) \rangle_{p(d|\theta)} - \theta \simeq \theta \left(\frac{N\epsilon^2}{3\sigma^2} - 1 \right), \quad (\text{C13})$$

which is very significant (the estimator clusters near zero, no matter the value of θ because of the symmetry of the prior). The variance of the estimator T in this limit is

$$\text{cov}(T, T) \simeq \frac{\epsilon^4}{9\sigma^4} \text{cov}(D, D) = N \frac{\epsilon^4}{9\sigma^2}. \quad (\text{C14})$$

Note that $\epsilon^2/3$ is the variance of the prior distribution, so the variance of our estimator is much smaller than that of the prior⁴. Note that the posterior mean is not a particularly useful estimator when the prior is so narrow, since the posterior is dominated by the prior rather than the data, and is roughly uniform in $[-\epsilon, \epsilon]$ while vanishing outside this interval. While the posterior mean is always close to zero, this carries little information about the true parameter value beyond what is contained in the prior.

The Fisher information for our likelihood function is

$$I(\theta) = \frac{N}{\sigma^2}. \quad (\text{C15})$$

In both the wide-prior ($\epsilon \gg \sigma/\sqrt{N}$) and narrow-prior ($\epsilon \ll \sigma/\sqrt{N}$) cases, the Cramer-Rao bound is satisfied. For the wide prior case, we have

$$T(d) \simeq \frac{D}{N}, \quad (\text{C16})$$

whence

$$\text{cov}(T, T) = \frac{\sigma^2}{N} \geq \frac{1}{I(\theta)} = \frac{\sigma^2}{N}. \quad (\text{C17})$$

In the wide-prior limit, we achieve the Cramer-Rao bound! For the narrow-prior case, we have significant bias. The numerator of the Cramer-Rao bound, Eq. (A9), is

$$\frac{\partial\psi}{\partial\theta} + \frac{\partial b}{\partial\theta} \simeq 1 + \frac{N\epsilon^2}{3\sigma^2} - 1 = \frac{N\epsilon^2}{3\sigma^2}. \quad (\text{C18})$$

The full Cramer-Rao bound is

$$\text{cov}(T, T) \geq \frac{(\partial\psi/\partial\theta + \partial b/\partial\theta)^2}{I(\theta)} = N \frac{\epsilon^4}{9\sigma^2}. \quad (\text{C19})$$

Comparing with Eq. (C14), we see that we achieve the Cramer-Rao bound in the narrow-prior limit, too!

As an aside, in the narrow prior limit, the variance of the posterior, Eq. (C4), is

$$\int d\theta \left(\theta - \langle \theta' \rangle_{p(\theta'|d)} \right)^2 p(\theta|d) = \frac{\epsilon^2}{3} + \mathcal{O}(\epsilon^4), \quad (\text{C20})$$

which is much larger than the variance of the estimator (since the estimator clusters near zero, while the posterior is approximately the prior in the narrow-prior limit).

Assuming that the prior is correct (that is, that the true value of θ , denoted by θ_0 , is between $\pm\epsilon$), an estimate based on the mean of the posterior exhibits lower standard error than an estimate based on the sample mean. The standard error for an estimator is defined as

$$\text{se}(T(d)) \equiv \sqrt{\left\langle (T(d) - \theta_0)^2 \right\rangle_{p(d|\theta_0)}} \quad (\text{C21})$$

$$= \sqrt{\text{cov}(T, T) + b^2(\theta_0)}. \quad (\text{C22})$$

When the priors are wide, the mean of the posterior is approximately equal to the sample mean, and the standard error is then the sample variance; when the priors are narrow, the posterior mean is nearly 0, which is always within $\pm\epsilon$ of the true value of θ , so the standard error is $\sim \epsilon$, which is much smaller than the variance of the sample mean. In both cases, the effect of the prior is to produce a more accurate (but biased!) estimate of the parameter than can be achieved using the sample mean alone.

⁴Be careful! The variance of the prior is an integral over the parameter θ , while the variance of the estimator refers to the variance at fixed θ under repeated noise realizations.